

Distinct distributions of elliptical and disk galaxies across the Local Supercluster as a Λ CDM prediction

Received: 10 March 2023

Accepted: 16 October 2023

Published online: 20 November 2023

 Check for updatesTill Sawala^{1,2}✉, Carlos Frenk², Jens Jasche^{3,4}, Peter H. Johansson¹ & Guilhem Lavaux⁴

Galaxies of different types are not equally distributed in the Local Universe. In particular, the supergalactic plane is prominent among the brightest ellipticals, but inconspicuous among the brightest disk galaxies. This striking difference provides a unique test for our understanding of galaxy and structure formation. Here we use the SIBELIUS DARK constrained simulation to confront the predictions of the standard Lambda Cold Dark Matter (Λ CDM) model and standard galaxy formation theory with these observations. We find that SIBELIUS DARK reproduces the spatial distributions of disks and ellipticals and, in particular, the observed excess of massive ellipticals near the supergalactic equator. We show that this follows directly from the local large-scale structure and from the standard galaxy formation paradigm, wherein disk galaxies evolve mostly in isolation, while giant ellipticals congregate in the massive clusters that define the supergalactic plane. Rather than being anomalous as earlier works have suggested, the distributions of giant ellipticals and disks in the Local Universe and in relation to the supergalactic plane are key predictions of the Λ CDM model.

The Local Supercluster is the largest structure in the Local Universe¹; it defines the supergalactic plane and the supergalactic coordinate system^{2,3}. While the plane was originally defined by the relatively nearby clusters such as Virgo and Fornax, it is now understood to extend to at least redshift $z = 0.02$ as an excess of bright elliptical and radio galaxies near the supergalactic equator^{4–6}. Strikingly, however, there is no corresponding excess in bright disk galaxies^{7,8}.

In the standard paradigm of hierarchical structure formation⁹, denser regions are characterized by a greater abundance of dark matter haloes and, in particular, more massive ones¹⁰. Standard galaxy formation theory predicts that disk galaxies evolve largely in isolation, growing primarily through in-situ star formation fuelled by the continuous accretion of gas^{11,12}. By contrast, the higher ambient temperature in denser regions restricts the gas supply into haloes, which leads to gas depletion and the eventual quenching of star formation. Denser

regions are also characterized by a higher merger rate and a higher fraction of gas-poor mergers, both of which are understood to lead to the formation of elliptical galaxies^{13,14}.

However, the metamorphosis of galaxies is believed to take hundreds of millions of years, precluding its direct observation in individual objects. The differing distributions of galaxies of different types and masses in different environments within the Local Universe thus provide an important opportunity to simultaneously test the ability of the cosmological framework to explain the observed large-scale structure and to enhance our understanding of galaxy formation.

A Local Universe constrained simulation

Direct comparisons of model predictions to observations in the Local Universe require a constrained simulation^{15–19}. In this work, we use the

¹Department of Physics, University of Helsinki, Helsinki, Finland. ²Institute for Computational Cosmology, Durham University, Durham, UK. ³The Oskar Klein Centre, Department of Physics, Stockholm University, Albanova University Center, Stockholm, Sweden. ⁴CNRS & Institut d'Astrophysique de Paris, Sorbonne Université, Paris, France. ✉e-mail: till.sawala@helsinki.fi

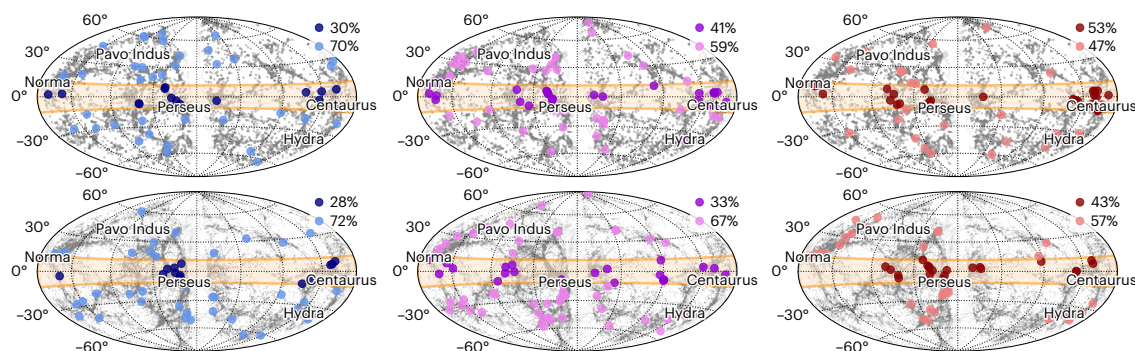


Fig. 1 | Distributions of disks, intermediates and ellipticals in the Local Universe up to $z = 0.02$. Hammer projection in supergalactic coordinates of the distribution of the most massive disks (left), intermediates (centre) and ellipticals (right) in the redshift range of $0.01 < z < 0.02$, as reported in the 2MRS survey (top) and as modelled in SIBELIUS (bottom). The shaded areas correspond to $|\sin(\text{SGB})| < 0.2$ ($-11.5^\circ \leq \text{SGB} \leq 11.5^\circ$) around the supergalactic equator.

Dark and light symbols show individual galaxies that lie inside and outside this region, respectively, and percentages in the top right of each panel express their relative numbers. Grey points denote lower mass galaxies (fainter for $|b| < 10^\circ$) irrespective of morphology; labels indicate the positions of five galaxy clusters. In both the 2MRS data and the SIBELIUS simulation, a significantly higher fraction of massive ellipticals than of massive disks lie close to the supergalactic plane.

SIBELIUS DARK (SIBELIUS) simulation¹⁹ that is designed to reproduce the galaxy distribution out to a comoving distance of ~ 200 Mpc (with $z \approx 0.04$). The initial conditions are constrained using the Bayesian Origin Reconstruction from Galaxies (BORG) algorithm^{20–22} to represent the most likely initial conditions that give rise to the observed large-scale structure in the 2M++ galaxy redshift survey²³, in the Lambda Cold Dark Matter (Λ CDM) cosmology, with parameters for dark energy fraction $\Omega_\Lambda = 0.693$, all-matter fraction $\Omega_m = 0.307$, baryonic matter fraction $\Omega_b = 0.04825$, 8 Mpc matter density fluctuations $\sigma_8 = 0.8288$, primordial density fluctuation spectral index $n_s = 0.9611$ and the Hubble Constant $H_0 = 67.77 \text{ km s}^{-1} \text{ Mpc}^{-1}$.

To predict the SIBELIUS galaxy population, accounting for the environment and merger history, the semi-analytical galaxy formation model GALFORM^{24,25} was applied to its halo merger tree. In GALFORM, galaxy properties such as the stellar mass and morphology are calculated based on the properties of the evolving dark matter structures, such as mass, accretion rate, spin and mergers, with analytical prescriptions for processes including gas cooling, star formation, stellar evolution, black hole formation, feedback from supernovae and active galactic nuclei (AGN), dynamical friction and dynamical instabilities. Mergers (particularly major mergers) and starbursts caused by disk instabilities are the primary processes that can lead to the growth of the elliptical-defining bulge and the transformation of a disk galaxy into an elliptical galaxy²⁴.

Of particular relevance to this study is that the BORG algorithm used in the construction of the constraints is agnostic to the astrophysical processes that may give rise to the divergent formation pathways of disks and ellipticals, while the GALFORM model is agnostic to the particular structures present in the Local Universe, which, however, determine the properties of the merger trees.

We classify the SIBELIUS galaxies according to their bulge-to-disk mass ratio, B/D , with distribution as shown in Extended Data Fig. 1. We designate those with $B/D < 1/4$ as disk galaxies, those with $1/4 < B/D < 8$ as intermediates and those with $B/D > 8$ as ellipticals²⁶. As shown in Extended Data Fig. 2, our results are not sensitive to these particular choices. We focus here mostly on the distributions of disks and ellipticals, which are the subjects of refs. 8, 27, but the intermediates provide a further point of comparison.

Predicted and observed distributions

For comparison to the observations and, in particular, to the results of ref. 27, we select from the Two Micron All Sky Survey (2MASS) galaxy redshift catalogue²⁸ (2MRS) the brightest objects in the redshift range

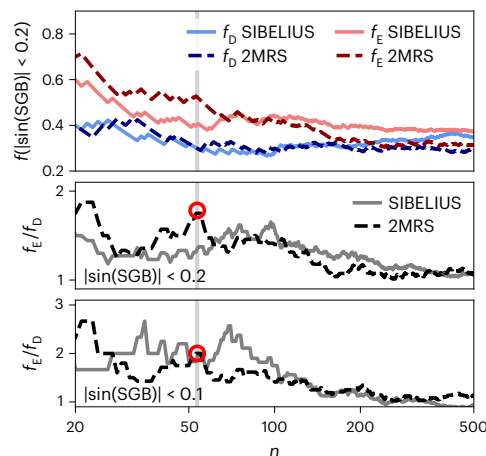


Fig. 2 | Excess of ellipticals relative to disks, as a function of sample size. Top, the fraction of the most massive n disks (f_D) and the most massive n ellipticals (f_E) in SIBELIUS and 2MRS at $0.01 < z < 0.02$, located at $|\sin(\text{SGB})| < 0.2$. Middle, f_E/f_D , the fraction of the most massive n ellipticals divided by the fraction of the most massive n disks at $|\sin(\text{SGB})| < 0.2$. Bottom, ratio f_E/f_D , but now for $|\sin(\text{SGB})| < 0.1$. As indicated by the red circles, the values of f_E/f_D in 2MRS peak at the value of n chosen in ref. 27.

$0.01 < z < 0.02$ by absolute K-band magnitude. Excluding objects with absolute galactic latitude $|b| < 10^\circ$ and applying a magnitude limit of $M_K < -25.19$, we obtain an identical sample of galaxies composed of 54 disks, 53 ellipticals and 73 intermediates.

In Fig. 1, we compare the distributions in supergalactic coordinates as reported in 2MRS, at the top, and as calculated by SIBELIUS, at the bottom. From left to right, diagrams show the positions of the most massive $n = 54$ disks (in blue), $n = 73$ intermediates (in purple) and $n = 53$ ellipticals (in red). In all diagrams, grey dots show the positions of fainter galaxies tracing the local large-scale structure. Also shown are the locations of five galaxy clusters in this redshift range. Orange lines enclose a region of supergalactic latitude (SGB) defined by $|\sin(\text{SGB})| < 0.2$ ($-11.5^\circ \leq \text{SGB} \leq 11.5^\circ$) around the supergalactic plane. Galaxies within and outside this region are denoted by dark and light symbols, respectively.

In both 2MRS and SIBELIUS, the fraction of galaxies close to the supergalactic equator depends on their type. This fraction increases from disks to intermediates to ellipticals; the most massive ellipticals

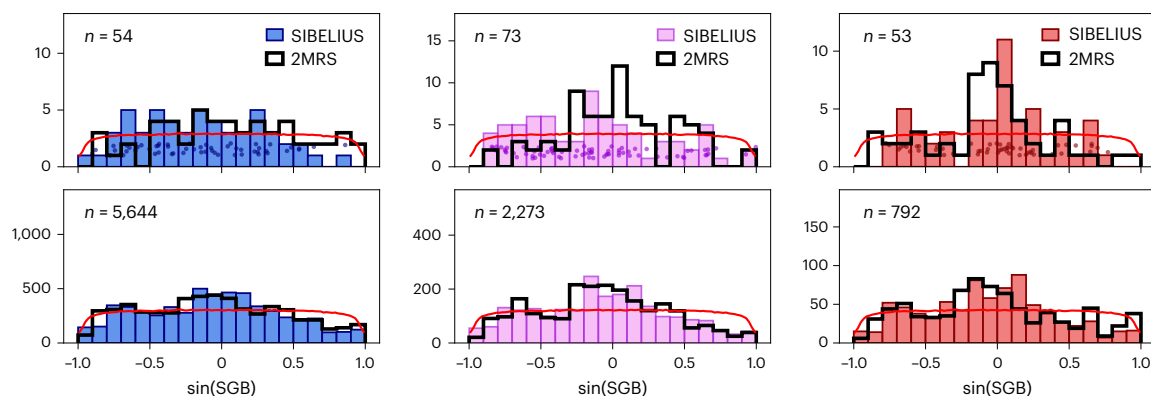


Fig. 3 | Distributions of SGB in the redshift range $0.01 < z < 0.02$ for galaxies of different morphology. Disks are shown on the left, intermediates in the middle and ellipticals on the right. In each case, galaxies with $|b| < 10^\circ$ are excluded. Histograms show the 2MRS data and results from SIBELIUS. The top row shows the n most massive objects in each class to match the samples of ref. 27, the bottom row shows the full 2MRS samples in this redshift range. In each case, we compare to an equal number of objects from SIBELIUS. Red

lines show the isotropic expectation accounting for sky coverage. In both the observations and the simulation, the concentration toward the supergalactic equator is much more prominent in the most massive ellipticals than in the most massive disks; intermediates fall in between. By contrast, for the larger sample sizes, the distributions of different galaxy types do not show this effect to such an extent.

are more strongly clustered than the most massive disks. We explore the origin of these differences in the next sections.

Due to the relatively small sample sizes, it is worth considering the possibility of a coincidence, or the ‘look elsewhere’ effect. In Fig. 2, we compare the fractions of the most massive n disks f_D and the most massive n ellipticals f_E , at $|\sin(\text{SGB})| < 0.2$ in 2MRS and SIBELIUS, at $0.01 < z < 0.02$, as functions of n . Overall, we find good agreement between the simulation and the observations and a significant excess $f_E > f_D$ for all $n < 150$ (Note that at large n , completeness may affect the results). We also find that in 2MRS, the relative excess peaks at the values used by ref. 27. Comparisons at any other $n > 25$ yield a smaller relative excess, indicating the presence of a ‘look elsewhere’ effect. In both SIBELIUS and 2MRS, the relative excess increases for a narrower band of $|\sin(\text{SGB})| < 0.1$, albeit with even smaller sample sizes.

Drawing random subsamples of 50 out of each of the 100 most massive disks and ellipticals in SIBELIUS yields configurations where ellipticals are more clustered than disks (that is more objects within $|\sin(\text{SGB})| < 0.2$) in approximately 95.2% of cases. This number decreases slightly to 93.5% for $|\sin(\text{SGB})| < 0.25$ and to 84.5% for $|\sin(\text{SGB})| < 0.15$. For 2MRS, the corresponding numbers are 88.0%, 86.7% and 87.0%. The excess is equally significant in SIBELIUS and 2MRS.

In the top row of Fig. 3, we show the distributions of $\sin(\text{SGB})$ at $0.01 < z < 0.02$ for the same numbers of most massive disks (left), intermediates (middle) and ellipticals (right) as used by ref. 27. Black bars represent the 2MRS data, filled coloured bars represent SIBELIUS, for which points denote individual objects. As was already apparent from Figs. 1 and 2, we find a strong excess toward low supergalactic latitudes of the most massive ellipticals in SIBELIUS, in good agreement with 2MRS. There is a much weaker enhancement for the most massive disks, also in good agreement with observations. In both cases, the distributions of the most massive intermediates fall in between: they are more strongly clustered than the most massive disks, but less so than the most massive ellipticals.

When we expand our samples to match the respective sample sizes of the 2MRS catalogue, as shown in the bottom row of Fig. 3, we find broadly similar distributions for disks, intermediates and ellipticals and excellent agreement between the simulation and the observations. To assess the significance of the agreement of the SGB distributions in SIBELIUS and 2MRS, we generate random permutations of the observational data. This gives a probability for the conspicuous agreement in the bottom row of Fig. 3 to arise by chance of $< 0.001\%$ for

either disks or intermediates and $\sim 0.02\%$ for ellipticals (which have a smaller sample size).

The results of SIBELIUS thus reproduce those presented in ref. 27 derived from 2MRS: there is a clear difference in clustering between ellipticals and disks in relation to the supergalactic plane, but this is only manifest among the most massive objects, not in the much larger samples.

Causes of the separation

We identify several causes for the different distributions of the most massive disks and ellipticals in the SIBELIUS simulation and, by implication, in the Local Universe. We first note that the most massive ellipticals in SIBELIUS are much more massive than the most massive disks, and the most massive galaxies in SIBELIUS are overwhelmingly elliptical. For instance, while the 100 most massive disks in the range $0.01 < z < 0.02$ have a median stellar mass of $2.9 \times 10^{10} M_\odot$ (s.d. $0.8 \times 10^{10} M_\odot$), the corresponding figure for the 100 most massive ellipticals is $3.0 \times 10^{11} M_\odot$ (s.d. $1.7 \times 10^{11} M_\odot$), an order of magnitude higher.

In the left chart of Fig. 4, we compare the distributions of $\sin(\text{SGB})$ for galaxies of different stellar mass, irrespective of galaxy type. The most massive 10 or 100 galaxies, with stellar masses above $5 \times 10^{11} M_\odot$ and $2.5 \times 10^{10} M_\odot$, respectively, are significantly more concentrated toward low SGB than less massive galaxies.

This mass difference agrees with observational studies of galaxies in the Local Universe^{29–31}, which also find that the most massive galaxies are overwhelmingly elliptical. Using neutral atomic hydrogen and ultraviolet data, ref. 32 recently measured the fraction of ellipticals among galaxies with stellar masses above $10^{11.4} M_\odot$ to be $\sim 87\%$. Hydrodynamic simulations³³ and the GALFORM semi-analytical model, both of which are calibrated to reproduce the observed mass functions, qualitatively reproduce these findings. This suggests that the mass difference we identify in SIBELIUS reflects that in the real Universe and explains part of the difference in the distributions of $\sin(\text{SGB})$, in line with the standard model prediction³⁴ and observations³⁵ that more massive galaxies are more strongly clustered.

The K-band magnitudes in 2MASS for the most massive disks and ellipticals are in fact similar²⁷. We attribute this to the previously reported systematic underestimation of the magnitudes of massive ellipticals in 2MASS^{36–40}. Applying the correction suggested by ref. 39 to the ellipticals would result in a much larger fraction of ellipticals among the brightest galaxies, in line with the other studies mentioned

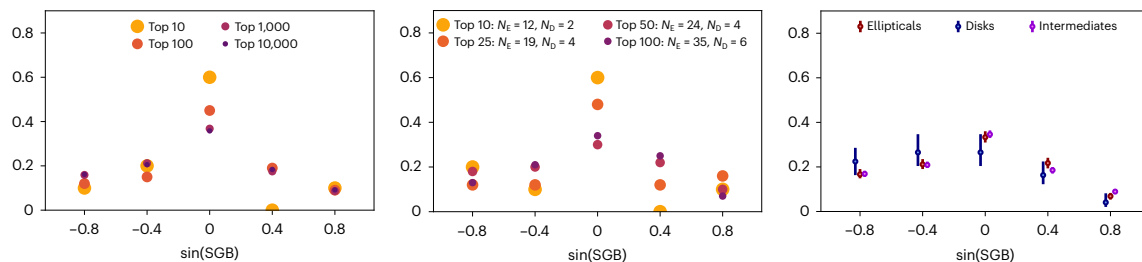


Fig. 4 | Distributions of SGB in the redshift range $0.01 < z < 0.02$ for simulated galaxies and host haloes, ranked according to different criteria. Left, distributions of galaxies ranked by stellar mass; the 10 or 100 most massive galaxies in the SIBELIUS simulation are significantly more concentrated to low supergalactic latitudes compared to less massive galaxies. The distributions of the 1,000 or 10,000 most massive galaxies are similar. Middle, distribution of the most massive haloes, ranked by M_{200} . The most massive haloes (which contain

a high number n_e of the 50 most massive ellipticals but a much lesser number n_D of the 50 most massive disks) are close to the supergalactic plane. Right, distributions of ellipticals, disks and intermediates in the mass range of the most massive 100 disks, that is, at the same stellar mass. Bars indicate $\pm 1\sigma$ statistical error. Even comparing at equal mass, ellipticals and intermediates are more strongly concentrated near the supergalactic plane than disk galaxies.

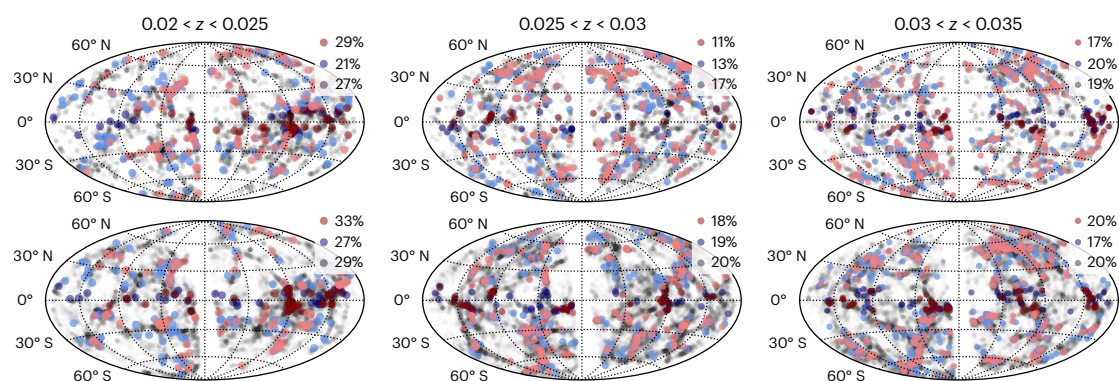


Fig. 5 | Distributions of galaxies beyond $z = 0.02$. Hammer projection in supergalactic coordinates of the distributions of the most massive disks (blue) and ellipticals (red) in 2MRS (top) and SIBELIUS (bottom) in three redshift slices. Galaxies are selected at $|b| > 10^\circ$ and with masses similar to the 100 most massive galaxies of each type for z in the range 0.01–0.02. As in Fig. 1, dark and faint circles denote galaxies within and outside $\pm 11.5^\circ$ of the supergalactic plane, respectively. Fainter galaxies are shown in grey. The percentages in the top right

of each panel express the fraction of galaxies in each class that are within $\pm 11.5^\circ$ of the supergalactic plane. The ellipticals more closely trace the distribution of the most prominent structures, while the disks are more equally distributed. The excess of galaxies at low supergalactic latitudes extends to $z \approx 0.025$. At higher redshifts, the distributions of both structures and galaxies are no longer aligned with the supergalactic plane.

above and with SIBELIUS. Of course, results based on ranking galaxies within the same morphological class remain unchanged.

We also find evidence that the different environments on or off the supergalactic plane act to separate the most massive galaxies by morphology, besides simply sorting them by mass. In the centre chart of Fig. 4, we show the distributions in $\sin(\text{SGB})$ of host haloes in different mass ranges. As expected, the most massive 10 or 25 haloes in SIBELIUS in this redshift range are strongly biased toward the supergalactic plane. They also host a significant number n_e of the 50 most massive ellipticals, but only a small number n_D of the 50 most massive disks. For example, 19 of the 50 most massive ellipticals but only 4 of the 50 most massive disks are in the 25 most massive haloes. The 50 most massive ellipticals reside in 45 haloes with a median mass of $M_{200} = 9.0 \times 10^{13} M_\odot$, while the 50 most massive disks are all in different haloes with a median mass of $M_{200} = 1.9 \times 10^{12} M_\odot$, over 50 times lower.

In the right chart of Fig. 4, we show the distribution of galaxies of the different types—ellipticals, disks and intermediates—in the mass range of the 100 most massive disks. All three galaxy samples have very similar masses, but the disk galaxies are still significantly less strongly clustered than ellipticals or intermediates of similar mass. This further emphasizes the role of the environment: galaxies of the same mass are less likely to evolve into massive disks in the dense environment that marks out the supergalactic plane.

In the Horizon-AGN hydrodynamical simulation, two scenarios for the formation of massive disk galaxies are identified³³: 1) an exceptionally quiet merger history or 2) a late merger of a spheroid with a massive, gas-rich satellite; both are less likely to occur in a dense environment, where mergers are more common and cold gas fractions are lower. This provides an additional explanation, an environmental explanation, for the relative paucity of massive disks near the supergalactic plane.

The extent of the supergalactic plane

That SIBELIUS is designed to reproduce structures out to ~ 200 Mpc also lets us investigate the extent of the supergalactic plane beyond $z = 0.02$. Figure 5 shows the sky distributions of disks and ellipticals in 2MRS (top) and SIBELIUS (bottom) in redshift shells out to $z = 0.035$.

The overdensity at low supergalactic latitudes only extends to $z \approx 0.025$. Beyond this, structures no longer align with the supergalactic plane, the distributions become less dominated by individual clusters and the fraction of galaxies near the equator fluctuates around the isotropic expectation value of $\sim 20\%$. However, in every redshift range, both in 2MRS and SIBELIUS, elliptical galaxies are more strongly clustered than disks. We also investigated the presence of assembly bias, that is, the difference in clustering that is not explained by halo mass⁴¹. However, as shown in Extended Data Fig. 3, we found no significant effect for the comparatively small galaxy samples we consider here.

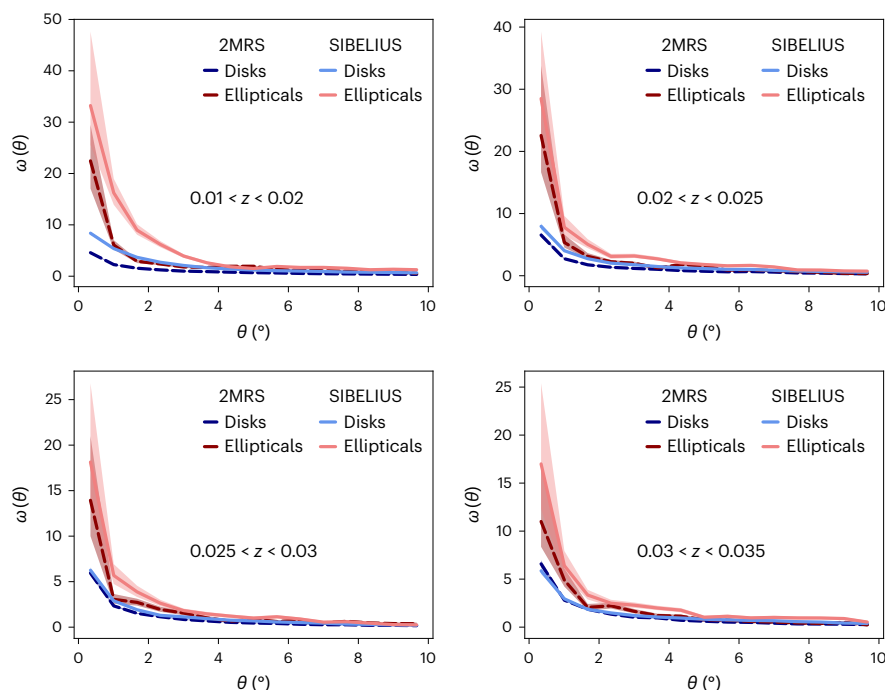


Fig. 6 | Angular correlation functions. The graph shows the angular correlation functions $\omega(\theta)$ of disks (blue) and ellipticals (red) in the SIBELIUS simulation (light solid lines) and the 2MRS data (dark dashed lines) in four redshift ranges. The top left chart corresponds to Fig. 1, while the top right chart and all bottom

charts correspond to Fig. 5. Shaded areas provide an estimate of the statistical uncertainty. In each redshift range within and beyond the Local Supercluster and in both 2MRS and SIBELIUS, elliptical galaxies show significantly stronger clustering than disks.

The enhanced clustering of ellipticals compared to disks also manifests in the angular correlation functions shown in Fig. 6. In both the simulation and the 2MRS data, and in every redshift range, ellipticals are significantly more clustered than the disks. The peculiar excess of massive ellipticals near the supergalactic plane at redshifts $0.01 < z < 0.02$ is not caused by exceptional galaxy formation physics but simply reflects the particular structures in this region.

Discussion

Constrained simulations such as SIBELIUS provide a unique window onto the local matter and galaxy distributions and allow powerful, direct tests of cosmological and astrophysical models. While environmental effects on morphology have been previously demonstrated^{42–46}, earlier works based on random environments rely on the assumption that cosmic variance will cancel out. By comparing theory and observations in matched environments, we do not have to make this assumption.

The SIBELIUS simulation, in combination with the GALFORM semi-analytical model, reproduces the distributions of ellipticals, intermediates and disks in the redshift range $0.01 < z < 0.02$ and beyond. Importantly, it also reproduces the striking difference in the clustering of the most massive ellipticals and disks in relation to the supergalactic plane.

We identify two causes for this dichotomy in SIBELIUS. First, the most massive ellipticals in the redshift range $0.01 < z < 0.02$ are much more massive than the most massive disks, and the clustering strength depends strongly on galaxy mass. Galaxies which fall between the ellipticals and disks in both morphology and stellar mass also follow an intermediate spatial distribution. Second, from the fact that the most massive disks are less strongly clustered than intermediates or ellipticals of the same mass, we conclude that the environment prevailing in the supergalactic plane inhibits the conditions necessary for massive disk formation: a quiet merger history and the continuous supply of cold gas. In SIBELIUS, a large fraction of the most massive ellipticals are

close to the supergalactic plane by virtue of residing within the galaxy clusters that define it.

The GALFORM galaxy formation model is idealized and cannot capture the full complexity of astrophysical processes at play in hydrodynamic simulations, let alone in the real universe. Nevertheless, it is patently sufficient to reproduce the distinct populations of elliptical and disk galaxies observed in the Local Universe.

The strikingly different distributions of bright ellipticals and disks in relation to the supergalactic plane do not require physics beyond the standard model. They arise naturally in the Λ CDM framework and the standard model of galaxy formation represented by the SIBELIUS simulation of the Local Universe. They are a direct consequence of the differences in mass and in the associated bias and of the transformation of disks into ellipticals within the clusters that define the supergalactic plane. Rather than as an anomaly, the observed distributions emerge as a prediction of the Λ CDM paradigm and as an important benchmark for any alternatives.

Methods

The SIBELIUS DARK simulation

Our work is based on the SIBELIUS simulation, a collisionless cosmological simulation which embeds a high-resolution constrained region of radius ~ 200 Mpc centred on the Local Group within a 1 Gpc^3 periodic volume. SIBELIUS is set up with cosmological parameters $\Omega_\Lambda = 0.693$, $\Omega_m = 0.307$, $\Omega_b = 0.042825$, $\sigma_8 = 0.8288$, $n_s = 0.9611$ and $H_0 = 67.77 \text{ km s}^{-1} \text{ Mpc}^{-1}$. The high-resolution region is sampled with approximately 130 billion dark matter particles of mass $1.15 \times 10^7 M_\odot$ with a maximum physical softening length of 1.4 kpc. More details of the numerical setup are given in ref. 19, which also includes additional comparisons with observations.

The initial conditions for SIBELIUS are created using white noise fields obtained through the BORG algorithm^{20–22}, which takes as an input the observed three-dimensional density field, inferred from the 2M++ galaxy survey²³. BORG is designed to infer the most likely initial

configuration that gave rise to the input galaxy density distribution, subject to the specified cosmology and an assumed galaxy bias model; it represents the most likely underlying matter distribution and formation history of the structures in the Local Universe. It is important to note, however, that the input galaxy distribution used in constructing the initial conditions for SIBELIUS does not differentiate by galaxy morphology or colour. The reproduction of the observed local large-scale structure is thus ‘by construction’, but the reproduction of distinct galaxy subpopulations is not.

Outputs of SIBELIUS are stored 200 times between $z = 25$ and $z = 0$. For each of these snapshots, haloes and subhaloes are respectively identified using a Friend-of-Friend algorithm and the Hierarchical-Bound-Tracing algorithm⁴⁷. Subhaloes are further processed into a merger tree, to which the GALFORM semi-analytical model is applied, as discussed below.

The GALFORM semi-analytical model

SIBELIUS only traces the evolution of matter via gravity. To derive a prediction for the galaxy population that can be compared to observations, the separate evolution of baryons and the formation of galaxies is followed using the semi-analytical model GALFORM. All semi-analytical models make the same basic assumptions: that baryons follow the accretion of matter (including its angular momentum) onto collapsed dark matter haloes⁴⁸ and that the evolution of baryons inside dark matter haloes and during mergers and interactions can be described by a set of coupled, non-linear differential equations^{9,49,50}. In GALFORM, these equations describe and account for various astrophysical processes including gas cooling, dynamical friction, star formation, stellar evolution, black hole formation and evolution and the formation and feedback from AGN, stars and supernovae.

The parameters of the model are set either from ab initio considerations, or via calibration to observations of the galaxy population. Since its first introduction²⁴ and through several subsequent updates^{10,25,51}, when applied to Λ CDM merger trees, GALFORM has been shown to reproduce many of the observed properties of the galaxy population, such as the neutral atomic hydrogen or stellar mass functions, the ratio of ellipticals to disks and the Tully–Fisher relation. It has also been shown to reproduce the galaxy population and the properties of individual galaxies (albeit with considerable scatter) in the EAGLE hydrodynamic simulation⁵². The version of GALFORM used for SIBELIUS²⁵ incorporates different initial stellar mass functions during starbursts, feedback that suppresses gas cooling in massive haloes and a new empirical star formation law in galaxy disks based on molecular gas content. While it still lacks some of the complexity of a full hydrodynamic simulation, GALFORM implements our current understanding of galaxy formation physics.

Importantly, the calibration of its free parameters has been performed using merger trees from randomized initial conditions without consideration of galaxy clustering²⁵ and independently of the constraints used in SIBELIUS, or of the particular structures present in the Local Universe.

Separation of disks, ellipticals and intermediates. As shown in Extended Data Fig. 1, the GALFORM semi-analytical model results in a bimodal distribution of galaxy morphologies as characterized by the bulge-to-disk mass ratio B/D , or equivalently, bulge-to-total mass ratio B/T . We use B/D to classify SIBELIUS galaxies into disks, ellipticals and intermediates. By default, we designate galaxies with $B/D < 1/4$ as disks, those with $1/4 < B/D < 8$ as intermediates and those with $B/D > 8$ as ellipticals²⁶. These two limits are indicated by dotted vertical lines in Extended Data Fig. 1. Using these values, 90% of disks have $B/D < 0.13$, while 90% of ellipticals have $B/D > 12.6$, indicative of a strongly bimodal distribution. It can also be seen that the morphology distribution depends on mass. In agreement with observations^{53,54}, the lower mass galaxy population contains a larger fraction of disks, while higher mass galaxies are more likely to be elliptical.

Because the thresholds separating the three classes are still somewhat arbitrary, we also investigate the effect of choosing different values. In Extended Data Fig. 2, we repeat Fig. 2 using $B/D < 1/A$ for disks and $B/D > A$ for ellipticals, for values of $A = 3, 4, 5$ and 6 . The behaviour, in terms of an excess clustering of the most massive ellipticals relative to disks, is similar in every case, demonstrating that our results are not sensitive to the precise delineation between galaxy types.

The Two Micron All Sky Survey redshift catalogue

The observed distributions of galaxies are drawn from the 2MRS²⁸ catalogue, which lists 44,599 galaxies. We include in our analysis all galaxies for which redshift and morphological types are available. Galaxy morphologies are as assigned in ref. 28, and we follow Peebles’ classification, whereby types ≥ 1 are classified as ‘spirals’ or ‘disks’, and types ≤ -5 are classified as ‘ellipticals’. We additionally identify intermediate types as ‘intermediates’.

To sort galaxies by luminosity, we infer absolute K-band magnitudes using the distance modulus. We adopt $H_0 = 70 \text{ km s}^{-1} \text{ Mpc}^{-1}$ for consistency with ref. 27, but we obtain the same galaxy samples with a value of $H_0 = 67.77 \text{ km s}^{-1} \text{ Mpc}^{-1}$ as used in the SIBELIUS simulation. We also adopt the same galactic latitude threshold $|b| > 10^\circ$ to obtain, from the 180 brightest galaxies in the redshift range $0.01 < z < 0.02$, the same samples of 54 brightest disks and 53 brightest ellipticals. We classify the remaining 73 as intermediates. We use the same morphology definitions and galactic latitude thresholds also at higher redshifts, up to $z \approx 0.035$, and we apply the same galactic latitude cuts to the simulation data.

To perform the comparison in redshift space, we use the measured redshifts for the 2MRS sample and use a value of $H_0 = 67.77 \text{ km s}^{-1} \text{ Mpc}^{-1}$ (in addition to the proper motions) when assigning redshifts to the galaxies in SIBELIUS based on their comoving simulation coordinates.

Magnitude bias for ellipticals. As noted by Peebles, the absolute K-band magnitudes of the brightest 53 disk galaxies and the brightest 54 elliptical galaxies at $0.01 < z < 0.02$ in 2MRS are similar, which would indicate similar stellar masses⁵⁵. This is in contrast to other observations, to the results of hydrodynamic simulations and also to the results of the GALFORM semi-analytical model, according to which the most massive ellipticals are significantly more massive than the most massive disks and, by implication, the most massive galaxies are overwhelmingly elliptical. We attribute this difference to the known fact that 2MASS systematically and significantly underestimates the luminosity of bright bulges and ellipticals^{36–40}.

In particular, by comparison to deeper K-band observations of the same objects³⁹, the finding was that 2MASS underestimates the luminosity of ellipticals and bulges by an average of 0.34 magnitudes, with the effect increasing for bright ellipticals. Applying a (somewhat conservative, but also crude) correction of -0.34 to the magnitudes of all ellipticals changes the distribution of morphological types among the brightest galaxies. Using the same selection as ref. 27, among the 180 brightest galaxies in 2MRS with $0.01 < z < 0.02$ and $|b| > 10^\circ$, the number of ellipticals increases from 53 to 89, while the number of disks decreases from 54 to 34. Among the brightest 100 galaxies, the number of ellipticals increases from 36 to 56, while the number of disks decreases from 25 to 14.

It is important to note that this correction would not change the ordering of galaxies within the same class; the identity and positions of the brightest n ellipticals and the brightest n disks remain the same. We have no need to apply a magnitude correction in this work, but its effect may explain why, when the 2MASS K-band magnitudes were taken at face value, stellar mass and the associated formation bias was excluded as a factor for explaining the different distributions of bright ellipticals and disks²⁷.

Angular correlation functions

As noted in the main text, the strikingly different distributions of bright ellipticals and disks in relation to the supergalactic plane reflects the

fact that, in the redshift range $0.01 < z < 0.02$, the Local Supercluster is the most prominent feature and aligns with the supergalactic equator. In other redshift ranges, we find no strong excess of ellipticals near the supergalactic plane, but as shown in Fig. 6, the difference between the correlation functions of disks and ellipticals persists at all redshifts, both in 2MRS and in SIBELIUS. The astrophysical processes that lead to different clustering of disks and ellipticals are universal, but the prominent excess of ellipticals at low supergalactic latitudes in the redshift range $0.01 < z < 0.02$ is caused by the presence of the Local Supercluster in this region of the Local Universe.

To compute the angular correlation functions $\omega(\theta)$, we use the Landy–Szalay estimator⁵⁶. For each redshift range and each galaxy type, we use the full 2MRS sample, choosing matching numbers of most massive galaxies in SIBELIUS and of random points. We apply the same $|b| > 10^\circ$ mask for each data set and for the random samples. We use the jackknife method to account for the random nature of galaxy formation in every data set and also repeat the random sampling to estimate the statistical uncertainty.

Assembly bias

Elliptical galaxies populate much more massive haloes than disk galaxies in our simulation. As is evident from Figs. 3 and 4, respectively, the stronger clustering of ellipticals toward the supergalactic plane for $0.01 < z < 0.02$ is present both when classifying galaxies by morphology and by host halo mass.

This may raise the question of whether the stronger clustering of ellipticals is driven entirely by the mass of their host haloes, or whether there is an additional effect, known as assembly bias⁴¹. Assembly bias can be measured by comparing the correlation functions of samples of galaxies separated by morphology to those obtained when the position of each galaxy in the sample is randomly assigned to a halo of similar mass, regardless of morphology. A systematic difference between the correlation function of the original sample and that of the shuffled counterpart must be attributable to factors other than halo mass, such as environment or assembly history; such difference is referred to as assembly bias. Ref. 41 found that assembly bias accounts for approximately 10% of the total bias, being positive for ellipticals, slightly negative for disks and decreasing in magnitude for the most massive galaxies.

We performed a similar test for the galaxy populations in SIBELIUS, showing the resulting angular correlation functions for different sample sizes of disks and ellipticals in Extended Data Fig. 3, for the same redshift ranges as in Fig. 6. When comparing to Fig. 6, it is important to note that because only central galaxies are considered, the correlation of galaxies within the same halo (the so-called one-halo term) is suppressed, resulting in weaker overall correlations.

In every case, as expected, we find a stronger correlation for the central ellipticals than for the central disks. There is some sign of positive assembly bias for our largest samples of galaxies ($n = 2,000$), but for smaller samples, the assembly biases can appear as both positive and negative and do not appear to be statistically significant.

We have no reason to believe that assembly bias does not also apply in the Local Universe, but it appears that the standard halo bias is the most significant effect in explaining the different distributions of the most massive disks and ellipticals with respect to the supergalactic plane.

Data availability

All data used in this work is publicly available. The 2MRS catalogue is provided in ref. 28. The halo and galaxy catalogues of the SIBELIUS simulation can be accessed via SQL at: <https://virgodb.dur.ac.uk>. SQL scripts to obtain the data used in this work are provided with our analysis code. The data is also available at <https://doi.org/10.6084/m9.figshare.22250602>.

Code availability

The analysis in this paper was performed in python3 and makes extensive use of open-source libraries, including Matplotlib v.3.7.0 (ref. 57), Scipy v.1.9.3 (ref. 58), NumPy v.1.23.5 (ref. 59), Astropy v.5.1.1 (ref. 60) and Corrfunc v.2.5.0 (ref. 61). A documented Jupyter notebook containing the code to reproduce all figures in this paper is available at: <https://github.com/TillSawala/supergalactic>.

References

- de Vaucouleurs, G. The distribution of bright galaxies and the local supergalaxy. *Vistas Astron.* **2**, 1584–1606 (1956).
- de Vaucouleurs, G., de Vaucouleurs, A. & Corwin, J. R. *Second Reference Catalogue of Bright Galaxies* (University of Texas Press, 1976).
- de Vaucouleurs, G. et al. *Third Reference Catalogue of Bright Galaxies* (Springer, 1991).
- Shaver, P. A. & Pierre, M. Large-scale anisotropy in the sky distribution of extragalactic radiosources. *Astron. Astrophys.* **220**, 35–41 (1989).
- Tully, R. B., Scaramella, R., Vettolani, G. & Zamorani, G. Possible geometric patterns in 0.1c scale structure. *Astrophys. J.* **388**, 9 (1992).
- Strauss, M. A. in *Sky Surveys. Protostars to Protogalaxies*, Vol. 43 (ed. Soifer, B. T.) 153–163 (Astronomical Society of the Pacific, 1993).
- Shaver, P. A. Radio surveys and large scale structure. *Aust. J. Phys.* **44**, 759 (1991).
- Peebles, P. J. E. The extended Local Supercluster. *Mon. Not. R. Astron. Soc.* **511**, 5093–5103 (2022).
- White, S. D. M. & Frenk, C. S. Galaxy formation through hierarchical clustering. *Astrophys. J.* **379**, 52 (1991).
- Benson, A. J., Cole, S., Frenk, C. S., Baugh, C. M. & Lacey, C. G. The nature of galaxy bias and clustering. *Mon. Not. R. Astron. Soc.* **311**, 793–808 (2000).
- Governato, F. et al. Forming disc galaxies in Λ CDM simulations. *Mon. Not. R. Astron. Soc.* **374**, 1479–1494 (2007).
- Guedes, J., Callegari, S., Madau, P. & Mayer, L. Forming realistic late-type spirals in a Λ CDM universe: the Eris simulation. *Astrophys. J.* **742**, 76 (2011).
- Naab, T., Johansson, P. H. & Ostriker, J. P. Minor mergers and the size evolution of elliptical galaxies. *Astrophys. J. Lett.* **699**, L178–L182 (2009).
- Johansson, P. H., Naab, T. & Ostriker, J. P. Forming early-type galaxies in Λ CDM simulations. I. Assembly histories. *Astrophys. J.* **754**, 115 (2012).
- Mathis, H. et al. Simulating the formation of the local galaxy population. *Mon. Not. R. Astron. Soc.* **333**, 739–762 (2002).
- Gottloeber, S., Hoffman, Y. & Yepes, G. Constrained Local Universe Simulations (CLUES). Preprint at <https://arxiv.org/abs/1005.2687> (2010).
- Libeskind, N. I. et al. The HESTIA project: simulations of the Local Group. *Mon. Not. R. Astron. Soc.* **498**, 2968–2983 (2020).
- Sawala, T. et al. The SIBELIUS project: e pluribus unum. *Mon. Not. R. Astron. Soc.* **509**, 1432–1446 (2022).
- McAlpine, S. et al. SIBELIUS-DARK: a galaxy catalogue of the local volume from a constrained realization simulation. *Mon. Not. R. Astron. Soc.* **512**, 5823–5847 (2022).
- Jasche, J. & Wandelt, B. D. Bayesian physical reconstruction of initial conditions from large-scale structure surveys. *Mon. Not. R. Astron. Soc.* **432**, 894–913 (2013).
- Lavaux, G. & Jasche, J. Unmasking the masked Universe: the 2M++ catalogue through Bayesian eyes. *Mon. Not. R. Astron. Soc.* **455**, 3169–3179 (2016).
- Jasche, J. & Lavaux, G. Physical Bayesian modelling of the non-linear matter distribution: new insights into the nearby universe. *Astron. Astrophys.* **625**, A64 (2019).

23. Lavaux, G. & Hudson, M. J. The 2M++ galaxy redshift catalogue. *Mon. Not. R. Astron. Soc.* **416**, 2840–2856 (2011).
24. Cole, S., Lacey, C. G., Baugh, C. M. & Frenk, C. S. Hierarchical galaxy formation. *Mon. Not. R. Astron. Soc.* **319**, 168–204 (2000).
25. Lacey, C. G. et al. A unified multiwavelength model of galaxy formation. *Mon. Not. R. Astron. Soc.* **462**, 3854–3911 (2016).
26. Benson, A. J. & Devereux, N. The origin of the Hubble sequence in Λ CDM cosmology. *Mon. Not. R. Astron. Soc.* **402**, 2321–2334 (2010).
27. Peebles, P. J. E. Anomalies in physical cosmology. *Ann. Phys. (N.Y.)* **447**, 169159 (2022).
28. Huchra, J. P. et al. The 2MASS Redshift Survey—description and data release. *Astrophys. J. Suppl. Ser.* **199**, 26 (2012).
29. Bernardi, M. et al. Early-type galaxies in the Sloan digital sky survey. I. The sample. *Astron. J.* **125**, 1817–1848 (2003).
30. Vulcani, B. et al. Galaxy stellar mass functions of different morphological types in clusters, and their evolution between $z=0.8$ and 0. *Mon. Not. R. Astron. Soc.* **412**, 246–268 (2011).
31. Ryan J, R. E. et al. The size evolution of passive galaxies: observations from the Wide-Field Camera 3 Early Release Science Program. *Astrophys. J.* **749**, 53 (2012).
32. Jackson, R. A. et al. Extremely massive disc galaxies in the nearby Universe form through gas-rich minor mergers. *Mon. Not. R. Astron. Soc.* **511**, 607–615 (2022).
33. Jackson, R. A. et al. Why do extremely massive disc galaxies exist today? *Mon. Not. R. Astron. Soc.* **494**, 5568–5575 (2020).
34. Kaiser, N. Clustering in real space and in redshift space. *Mon. Not. R. Astron. Soc.* **227**, 1–21 (1987).
35. Wake, D. A. et al. Galaxy clustering in the NEWFIRM Medium Band Survey: the relationship between stellar mass and dark matter halo mass at $1 < z < 2$. *Astrophys. J.* **728**, 46 (2011).
36. Lauer, T. R., Tremaine, S., Richstone, D. & Faber, S. M. Selection bias in observing the cosmological evolution of the M- σ and M-L relationships. *Astrophys. J.* **670**, 249–260 (2007).
37. Schombert, J. & Smith, A. K. The structure of galaxies I: surface photometry techniques. *Publ. Astron. Soc. Aust.* **29**, 174–192 (2012).
38. Kormendy, J. & Ho, L. C. Coevolution (or not) of supermassive black holes and host galaxies. *Annu. Rev. Astron. Astrophys.* **51**, 511–653 (2013).
39. Läsker, R., Ferrarese, L. & van de Ven, G. Supermassive black holes and their host galaxies. I. Bulge luminosities from dedicated near-infrared data. *Astrophys. J.* **780**, 69 (2014).
40. Ma, C.-P. et al. The MASSIVE Survey. I. A volume-limited integral-field spectroscopic study of the most massive early-type galaxies within 108 Mpc. *Astrophys. J.* **795**, 158 (2014).
41. Croton, D. J., Gao, L. & White, S. D. M. Halo assembly bias and its effects on galaxy clustering. *Mon. Not. R. Astron. Soc.* **374**, 1303–1309 (2007).
42. Zehavi, I. et al. The Luminosity and color dependence of the galaxy correlation function. *Astrophys. J.* **630**, 1–27 (2005).
43. Coil, A. L. et al. The DEEP2 Galaxy Redshift Survey: color and luminosity dependence of galaxy clustering at $z \sim 1$. *Astrophys. J.* **672**, 153–176 (2008).
44. Farrow, D. J. et al. Galaxy and mass assembly (GAMA): projected galaxy clustering. *Mon. Not. R. Astron. Soc.* **454**, 2120–2145 (2015).
45. Hatfield, P. W. et al. Comparing galaxy clustering in Horizon-AGN simulated light-cone mocks and VIDEO observations. *Mon. Not. R. Astron. Soc.* **490**, 5043–5056 (2019).
46. Smith, A., Cole, S., Grove, C., Norberg, P. & Zarrouk, P. A light-cone catalogue from the Millennium-XXL simulation: improved spatial interpolation and colour distributions for the DESI BGS. *Mon. Not. R. Astron. Soc.* **516**, 4529–4542 (2022).
47. Han, J., Jing, Y. P., Wang, H. & Wang, W. Resolving subhaloes’ lives with the Hierarchical Bound-Tracing algorithm. *Mon. Not. R. Astron. Soc.* **427**, 2437–2449 (2012).
48. White, S. D. M. & Rees, M. J. Core condensation in heavy halos: a two-stage theory for galaxy formation and clustering. *Mon. Not. R. Astron. Soc.* **183**, 341–358 (1978).
49. Cole, S., Aragon-Salamanca, A., Frenk, C. S., Navarro, J. F. & Zepf, S. E. A recipe for galaxy formation. *Mon. Not. R. Astron. Soc.* **271**, 781–806 (1994).
50. Baugh, C. M. A primer on hierarchical galaxy formation: the semi-analytical approach. *Rep. Prog. Phys.* **69**, 3101–3156 (2006).
51. Bower, R. G. et al. Breaking the hierarchy of galaxy formation. *Mon. Not. R. Astron. Soc.* **370**, 645–655 (2006).
52. Mitchell, P. D. et al. Comparing galaxy formation in semi-analytic models and hydrodynamical simulations. *Mon. Not. R. Astron. Soc.* **474**, 492–521 (2018).
53. Benson, A. J., Džanović, D., Frenk, C. S. & Sharples, R. Luminosity and stellar mass functions of discs and spheroids in the SDSS and the supermassive black hole mass function. *Mon. Not. R. Astron. Soc.* **379**, 841–866 (2007).
54. González, J. E., Lacey, C. G., Baugh, C. M., Frenk, C. S. & Benson, A. J. Testing model predictions of the cold dark matter cosmology for the sizes, colours, morphologies and luminosities of galaxies with the SDSS. *Mon. Not. R. Astron. Soc.* **397**, 1254–1274 (2009).
55. Kauffmann, G. & Charlot, S. The K-band luminosity function at $z=1$: a powerful constraint on galaxy formation theory. *Mon. Not. R. Astron. Soc.* **297**, L23–L28 (1998).
56. Landy, S. D. & Szalay, A. S. Bias and variance of angular correlation functions. *Astrophys. J.* **412**, 64 (1993).
57. Hunter, J. D. Matplotlib: a 2D graphics environment. *Comput. Sci. Eng.* **9**, 90–95 (2007).
58. Virtanen, P. et al. SciPy 1.0: fundamental algorithms for scientific computing in Python. *Nat. Methods* **17**, 261–272 (2020).
59. Harris, C. R. et al. Array programming with NumPy. *Nature* **585**, 357–362 (2020).
60. Astropy Collaboration et al. The Astropy Project: sustaining and growing a community-oriented open-source project and the latest major release (v5.0) of the core package. *Astrophys. J.* **935**, 167 (2022).
61. Sinha, M. & Garrison, L. H. CORRFUNC - a suite of blazing fast correlation functions on the CPU. *Mon. Not. R. Astron. Soc.* **491**, 3022–3041 (2020).

Acknowledgements

We sincerely thank P. J. E. Peebles for insightful discussions and guidance and T.S. thanks S. Räsänen for inspiring discussions. T.S. and P.H.J. acknowledge support from the Academy of Finland grant 339127. T.S. and C.S.F. are supported by the European Research Council (ERC) Advanced Investigator grant DMIDAS (GA 786910) and STFC Consolidated Grant ST/T000244/1. P.H.J. also acknowledges support from the European Research Council (ERC) Consolidator Grant KETJU (no. 818930). This work was also supported by the Simons Collaboration on ‘Learning the Universe’. This work used facilities hosted by the CSC—IT Centre for Science, Finland and the DiRAC@Durham facility, managed by the Institute for Computational Cosmology on behalf of the STFC DiRAC HPC Facility (www.dirac.ac.uk) and funded by BEIS capital funding via STFC capital grants ST/K00042X/1, ST/P002293/1, ST/R002371/1 and ST/S002502/1, Durham University and STFC operations grant ST/R000832/1. DiRAC is part of the UK National e-Infrastructure. This project used open-source software, including Matplotlib⁵⁷, SciPy⁵⁸, NumPy⁵⁹, Astropy⁶⁰ and Corrfunc⁶¹.

Author contributions

T.S. and C.F. developed the original ideas and T.S. performed the data analysis. J.J. and G.L. performed the reconstruction of the initial conditions for the SIBELIUS simulation, to which T.S., C.F., J.J., P.H.J.

and G.L. contributed jointly. T.S. wrote the first draft, and all co-authors edited and revised the manuscript.

Competing interests

The authors declare no competing interests.

Additional information

Extended data is available for this paper at <https://doi.org/10.1038/s41550-023-02130-6>.

Correspondence and requests for materials should be addressed to Till Sawala.

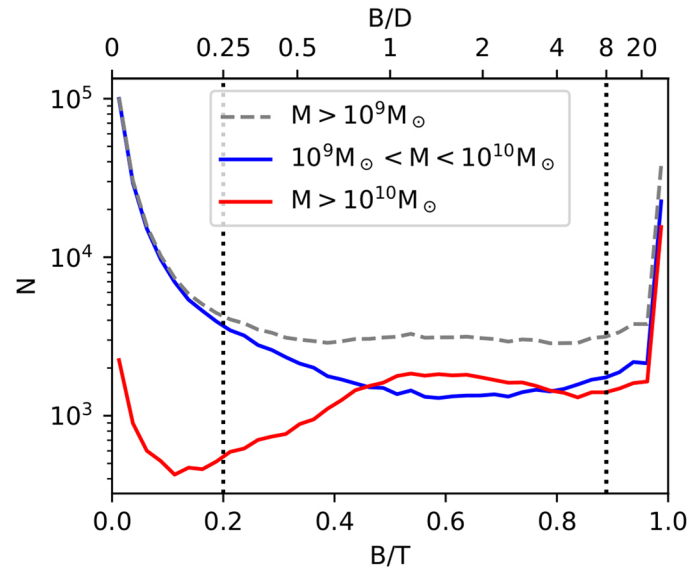
Peer review information *Nature Astronomy* thanks the anonymous reviewers for their contribution to the peer review of this work.

Reprints and permissions information is available at www.nature.com/reprints.

Publisher's note Springer Nature remains neutral with regard to jurisdictional claims in published maps and institutional affiliations.

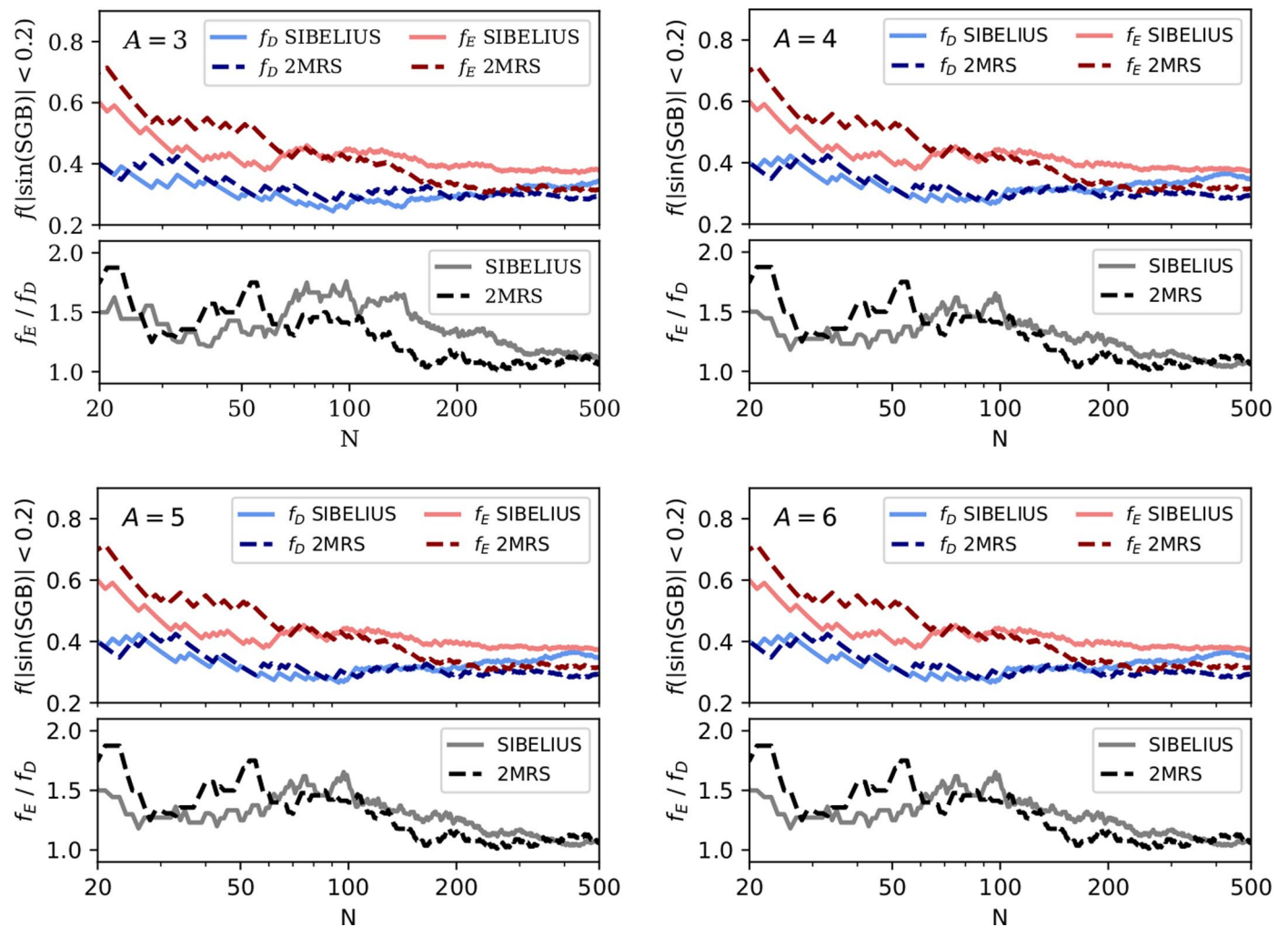
Open Access This article is licensed under a Creative Commons Attribution 4.0 International License, which permits use, sharing, adaptation, distribution and reproduction in any medium or format, as long as you give appropriate credit to the original author(s) and the source, provide a link to the Creative Commons license, and indicate if changes were made. The images or other third party material in this article are included in the article's Creative Commons license, unless indicated otherwise in a credit line to the material. If material is not included in the article's Creative Commons license and your intended use is not permitted by statutory regulation or exceeds the permitted use, you will need to obtain permission directly from the copyright holder. To view a copy of this license, visit <http://creativecommons.org/licenses/by/4.0/>.

© The Author(s) 2023



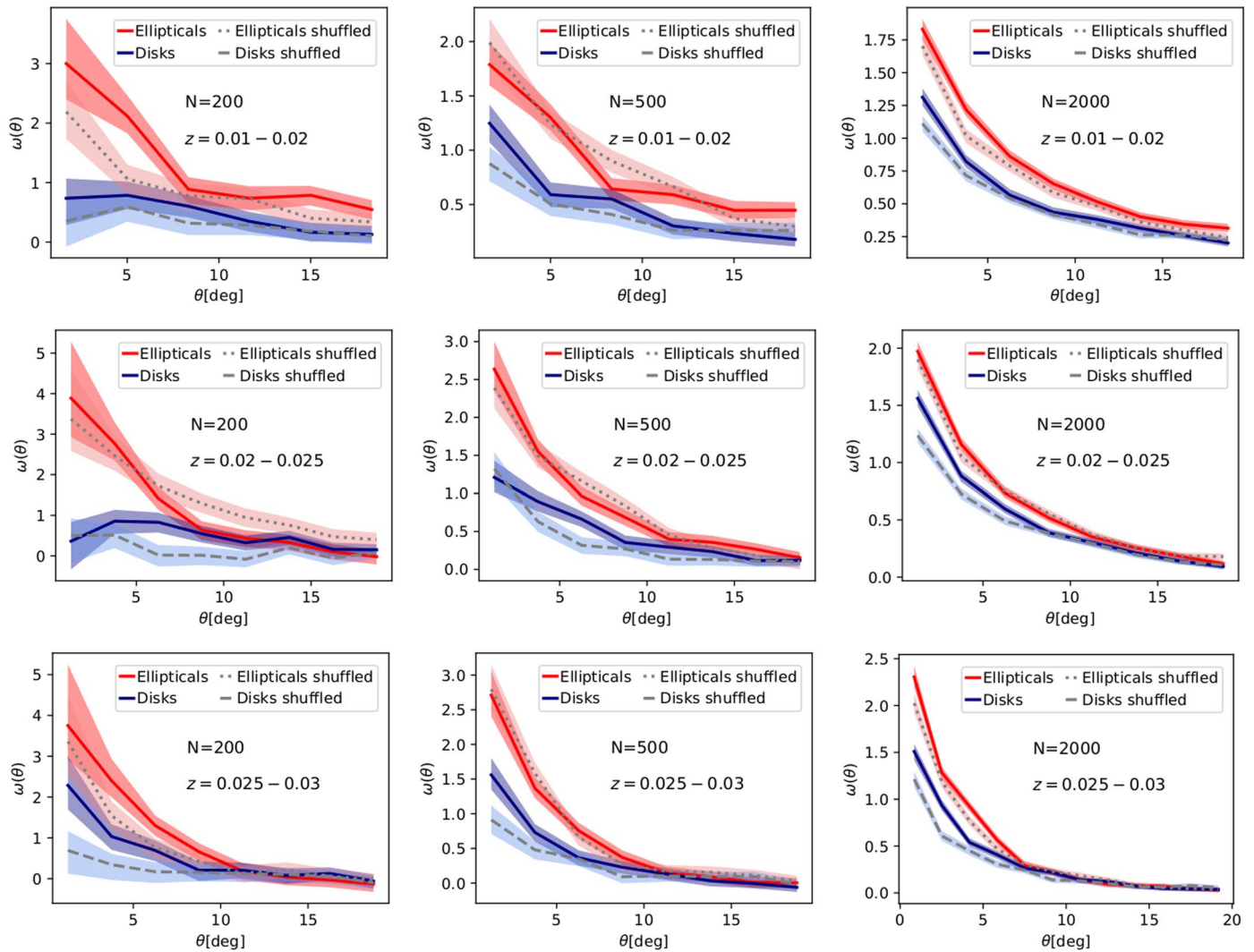
Extended Data Fig. 1 | Distribution of galaxy morphologies as parameterized by B/D or B/T in the Sibelius simulation in the redshift range $z = 0.01 - 0.04$. The blue curve shows galaxies in the stellar mass range $10^9 - 10^{10} M_{\odot}$, the red curve shows galaxies above $10^{10} M_{\odot}$, the grey dashed curve shows all galaxies above $10^9 M_{\odot}$. There is a clear bimodality in the bulge fraction, and the fraction of

galaxies with high bulge fraction increases with increasing stellar mass. The two vertical dotted lines denote $B/D = 1/4$ ($B/T = 1/5$), our default threshold separating disks and intermediates, and $B/D = 8$ ($B/T = 8/9$), our default threshold separating intermediates and ellipticals.



Extended Data Fig. 2 | The effect of adopting different thresholds to delineate disks, intermediates and ellipticals in Sibelius. Analogous to Fig. 2, each panel shows the excess of ellipticals and disks at $|\sin(\text{SGB})| < 0.2$, for different delineations between disks and ellipticals in Sibelius, as parameterized by bulge-to-disk ratios, less than $1/A$ for disks and greater than A for ellipticals.

The top row shows, from left to right, $A = 3$ and $A = 4$, while the bottom row shows $A = 5$ and $A = 6$. For reference, the 2MRS data is repeated on each panel. The greater abundance of ellipticals compared to disks at low supergalactic latitudes in Sibelius, and its dependence of N , is not sensitive to the particular choice of A .



Extended Data Fig. 3 | Assembly Bias. Angular correlation functions for samples of the N most massive central ellipticals and central disks in three redshift intervals, and for the corresponding 'shuffled' samples wherein each galaxy is replaced by another central galaxy of similar host halo mass regardless of galaxy

type. Note that the correlations are weaker than those in Fig. 6 due to the absence of the one-halo term. Assembly bias manifests itself as a difference between the original and shuffled samples, but we detect no clear effect of assembly bias for these sample sizes.